NRIAG Journal of Astronomy and Geophysics (2016) 5, 87–95

National Research Institute of Astronomy and Geophysics

NRIAG Journal of Astronomy and Geophysics

www.elsevier.com/locate/nrjag

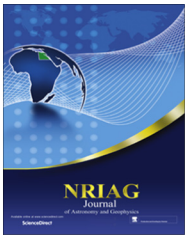

Seabed sub-bottom sediment classification using parametric sub-bottom profiler

Mohamed Saleh, Mostafa Rabah *

The National Research Institute of Astronomy & Geophysics, Egypt

Received 21 May 2015; revised 14 January 2016; accepted 20 January 2016
Available online 12 February 2016

KEYWORDS

Acoustic remote sensing;
Parametric sub-bottom profiler;
Sediment classification;
Physics based model

Abstract Many studies have been published concerning classification techniques of seabed surfaces using single beam, multibeam, and side scan sonars, while few paid attentions to classify sub-bottom layers using a non-linear Sub-Bottom Profiler (SBP). Non-linear SBP is known for its high resolution images due to the very short pulse length and aperture angle for high and low frequencies. This research is devoted to develop an energy based model that automatically characterizes the layered sediment types as a contribution step toward "what lies where in 3D?". Since the grain size is a function of the reflection coefficient, the main task is to compute the reflection coefficients where high impedance contrast is observed. The developed model extends the energy based surface model (Van Walree et al., 2006) to account for returns reflection of sub-layers where the reflection coefficients are computed sequentially after estimating the geo-acoustic parameters of the previous layer. The validation of the results depended on the model stability. However, physical core samples are still in favor to confirm the results. The model showed consistent stable results that agreed with the core samples knowledge of the studied area. The research concluded that the extended model approximates the reflection coefficient values and will be very promising if volume scatters and multiple reflections are included.

1. Introduction

The increased human marine activities in the offshore environment, such as wind farms, dredging operations, studies of marine geology and morphology have led to an imperative demand for accurate seafloor maps. These applications require knowledge of the seafloor topography and detailed information about the seafloor composition, both at the sediment surface and in deeper layers. The conventional approach to obtain information about the seafloor composition is to take physical sediment samples. This procedure is extremely expensive and time consuming. A much more attractive technique, which provides high spatial coverage at limited costs within short time, is acoustic remote sensing. Such technique has been successfully developed that classifies the seabed surfaces using single beam, multibeam, and side scan sonars (Van Walree et al.,

* Corresponding author.

Peer review under responsibility of National Research Institute of Astronomy and Geophysics.

ELSEVIER Production and hosting by Elsevier

http://dx.doi.org/10.1016/j.nrjag.2016.01.004

2006; Sternlicht Daniel and De Moustier Christian, 2003; Eleftherakis etal., 2012; Applied Physics Laboratory, 1994).

Underwater acoustic devices operate at frequencies between 10 Hz and 1 MHz. Frequencies lower than 10 Hz will penetrate deep into the seabed, whereas frequencies above 1 MHz get absorbed very quickly. Most systems used today for seabed mapping make use of a single acoustic frequency because different frequencies will require sophisticated sensor to capture the desired information (Anderson et al., 2008). Classical Sub-Bottom Profilers are single frequency sonars that aim to explore the first layers of sediments below the seafloor over a thickness commonly reaching several tens of meters. Sediment structure is directly observed by measuring the elapsed time of the received reflections of the acoustic energy when it encounters boundaries of different sediment layers.

Parametric SBPs are very compact transducers that exploit signal interference process to construct low frequency signal with a very narrow beam width $\pm 2°$. The consequence of such configuration is a very small footprint about 7% of water depth i.e. high spatial resolution. Basically, the transducer transmits two primary simultaneous high frequency signals that are slightly different e.g. 100–95 kHz at high sound pressure. Due to the high pressure, the sound propagation will be non-linear; water sound velocity is a function of water pressure, temperature, salinity, and density (Urick, 1982). The higher sound amplitudes will move faster than lower sound amplitudes. As a consequence, a number of secondary frequencies are produced such as harmonics, sums and difference of the emitted signals e.g. 100–95 = 5 kHz.

Acoustic remote sensing classification methods are numerous but can fall under two general categories: phenomenological approach and model based approach. Phenomenological approach is based on grouping echo like features together and labeling each group using the acquired ground truth samples. The aim is to extract some properties from the measured seabed echo that will allow the seabed to be classified into relatively homogeneous categories. Classifying the data in this way allows areas with similar seabed properties to be grouped together. The selection of grouping can be based on the similarity of amplitudes, skewness, energies, etc. This approach used the single beam echo sounder SBES echoes in Orłowski (1984) by grouping the square root ratio of the energy of second bottom echo to the first bottom echo. For the same device, Chivers et al. (1990), Heald and Pace (1996) and Siwabessy et al. (1999) grouped the energy summation of the first seabed echo tail and used it to represent the seabed roughness. Multibeam and side scan sonars echoes were also used by Preston et al. (2004) where the selective features were Mean, standard deviation, higher order moments, amplitude quintiles histogram and power spectral ratio. On the other hand, Hughes Clarke et al. (1997) exploited the Seabed backscatter strength.

Model based approach is a mathematical model to seek quantitative estimates of the geo-acoustic parameters that are incorporated in the model. This is achieved by modeling the received signal and optimizes its geo-acoustic parameters to match the acquired signal. Knowledge of transmitted pulse shape, duration, and power is needed. The unknown geo-acoustic parameters are estimated by minimizing the mismatch between the acquired and modeled acoustic signals. The advantage of this approach is that, in principle no independent measurements 'ground-truth' of the actual seabed is required. However, the ground truth is still recommended to assess the classification results. This approach is more complicated than the phenomenological approach since it requires full understanding of the physical process that the signal encounters.

2. Data description

The data consist of four sets of measurements that cover four areas characterized by various sediment types. The data used in this research were acquired by 'Innomar' in January 2007 in the Baltic Sea near Rostock. An SES-2000 standard SBP system is used for acquiring the data with filters set to a maximum bandwidth. The filter settings are experimental to ensure that the received signal is almost unchanged which consequently caused high noise level. Therefore, a filtering bandpass filter process is necessary to remove the presence of noise to increase the level of confidence within the analysis procedure.

Each area is acquired by four frequencies, the primary high frequency (± 100 kHz), and three secondary low frequencies $\pm(5, 10, 15$ kHz). Fig. 1 illustrates the echo prints of the four areas observed by the low 15 kHz. The first and second datasets, known as 'area 1' and 'area 2' have a survey length of 112 m and 128.5 m respectively with an average water depth of 20.5 m. The third survey line 'area 3' is approximately 118 m, with a starting water depth of 14 m that gradually increases to 15.5 m. Finally, 'area 4' is acquired over a survey length of 105.5 m and average water depth of 13 m. The acoustic survey for each survey is carried out at approximate speed of 10 km/h with ping rate of six pings/s.

A number of core samples were collected as ground truth. Unfortunately, no laboratory results were presented; however, the visual inspection indicated that 'area 1' and 'area 2' at the seabed surface are dominated by soft sediments, e.g. mud. 'Area 3' is dominated by medium mean grain size, e.g. sand, and 'area 4' is characterized by rough sediment such as pebble or rocks. The analysis done in this research will exploit the prior knowledge of sediment description as a guiding reference for the consistency of the classification results.

3. Time domain energy model

The nonlinear SBP can be considered as hybrid sonar system of SBES and classical SBP where the high frequency is also exploited to measure accurate seabed depth. As the transmitted acoustic signal travels downwards through the water column with a relative large beam width $\pm 30°$ such as in the case of SBES, the received energy will be a composite of reflections and backscatters from the seabed surface. On the contrary, nonlinear SBP operates with a very narrow beam width $\pm 1.8°$. This geometric configuration makes the received echo a function of the impedance contrast rather than interface micro roughness; 'SBP sees only echoes that come perpendicular from the seabed with very narrow beam width' (Lurton, 2002).

3.1. Seabed surface classification

The physics based model (Van Walree et al., 2006) describes the received echo energy as a function of the transmitted pulse energy, water column losses and seabed reflection. The aim here is to infer the sediment type from its reflection coefficient

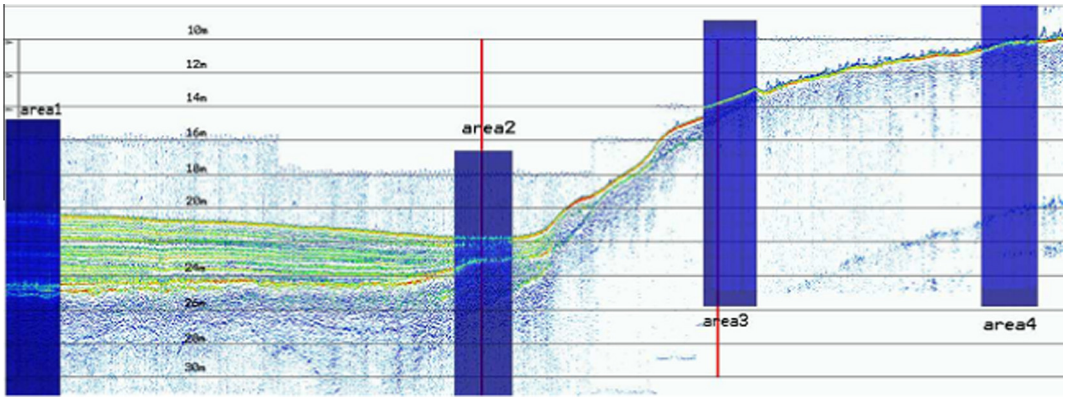

Figure 1 Echo print of sample profiler. The blue layers indicate the positions of the dataset.

by comparing it to the modeled reflection coefficient. This will be verified by computing the amount of energy received from a time window. Thus, the reflection coefficient can be estimated and correlated with Hamilton et al.'s (1982) sediment reflection coefficients (Garrison and Francois, 1879). Since the reflection coefficient is a function of sediment impedance, the results can then be inverted to the corresponding mean grain size. The reflection coefficient of measurements starts by extracting the signals from recordings. Then their envelopes are squared and integrated to yield echo energies. The received echo energy E_{RX} at a given direction 'receiver interface' and pulse duration is related to the transmitted pulse E_{TX} through:

$$E_{RX} = \frac{e^{(-4\alpha H)}}{4H^2} R^2 E_{TX} \tag{1}$$

where H denotes the distance between the echo sounder and the seafloor determined from the echo return time and the sound speed, and R is the reflection coefficient of the seabed surface. The energy is corrected for the spherical spreading factor $1/4H^2$ and the water absorption $e^{-4\alpha H}$. Water absorption is the exponential form that computes the absorption rate proportional to water depth, where α is the water absorption coefficient estimated from Francois and Garrison formulas (Hamilton et al., 1982) and converted to 1/m. From Eq. (1), the expression can now be inverted and the corresponding reflection coefficient of measurements can easily be estimated. The next step is to estimate the modeled reflection coefficients that correspond to the assumed sediment types (1φ till 9φ). This can be achieved via the sediment impedance, since it is a function of mean grain size $Z(M_z)''$. The mean grain size can be substituted by its geo-acoustic properties described via Bachman's regression equations that relate the sediment velocity and density to the mean grain size through (Siwabessy et al., 1999)

$$C_s = 1952 - 86.3M_z + 4.14M_z^2 \tag{2}$$

$$\rho_s = 2380 - 172.5M_z + 6.89M_z^2 \tag{3}$$

By combining Eqs. (2) and (3), sediment impedance Z_s (ρ_s c_s) can easily be estimated. One should note that although sediment impedance is uniquely identified as a function of the mean grain size, mean grain size as function of impedance $M_z(Z)$ gives various solutions. The link between the mean grain size and the echo energy is established via the Rayleigh reflection coefficient as follows:

$$R = (Z_s - Z_w)/(Z_s + Z_w) \tag{4}$$

The straightforward Eqs. (1)–(4) suffice to convert echo energies into mean grain size by equating the acoustic reflection coefficient in Eq. (1) to the model reflection coefficient in Eq. (4), provided that a calibration factor is available. Since the energy of the received echo E_{RX} is subject to an arbitrary scaling factor, a calibration factor C is required to calculate the R accordingly. Therefore, Eq. (1) can be rewritten as follows:

$$R = \frac{2CH}{e^{(-2\alpha H)}} \sqrt{E_{RX}} \tag{5}$$

where $C = 1/\sqrt{E_{TX}}$

With the prior knowledge of the general description of each area, the corresponding Rayleigh reflection coefficient at water–sediment surface can be determined using Hamilton and Bachman's Eqs. (2) and (3). The N calibration samples are associated with averaged mean grain size M_z that corresponds to its zones typically $M_z = 9\varphi$ for fines (area 1), $M_z = 8\varphi$ for (area 2), $M_z = 3\varphi$ for coarse (area 3), and $M_z = 0.5\varphi$ for very coarse (area 4). The number of calibration factors C_i per area can now be computed by matching the acoustic reflection coefficient of Eq. (5) to the expected Rayleigh reflection coefficient. By taking the root mean square of the C_i of each area we end up with four calibration factors. The calibration factors of area 1, 2 and 3 were very similar and slightly different at area 4 which could be due the high stochastic behavior of rough surface. Nevertheless, the four calibration factors are averaged and used for the entire dataset.

With the prior knowledge of the general description of each area, the corresponding Rayleigh reflection coefficient at water–sediment surface can be determined using Hamilton and Bachman's Eqs. (2) and (3). The N calibration samples are associated with averaged mean grain size M_z that corresponds to its zones typically $M_z = 9\varphi$ for fines (area 1), $M_z = 8\varphi$ for (area 2), $M_z = 3\varphi$ for coarse (area 3), and $M_z = -0.5\varphi$ for very coarse (area 4). The number of calibration factors C_i per area can now be computed by matching the acoustic reflection coefficient of Eq. (5) to the expected Rayleigh reflection coefficient. By taking the root mean square of the C_i of each area we end up with four calibration factors. The calibration factors of area 1, 2 and 3 were very similar and slightly different at area 4 which could be due the high stochastic behavior of rough surface. Nevertheless, for the sake

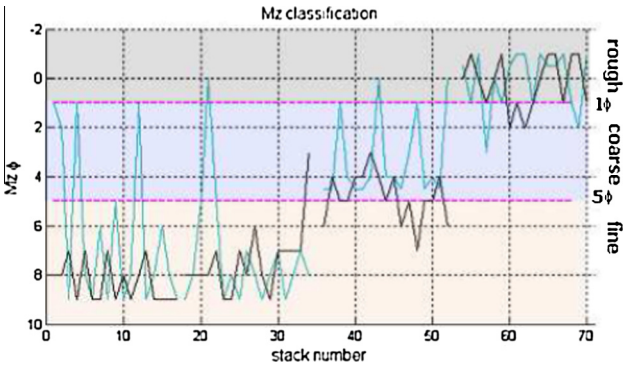

Figure 2 High frequency 100 kHz classification result using energy based model "Black solid" and APL model "Cyan solid". The vertical axis presents the main grain size. The horizontal axis presents the four areas in a sequential order area 1 = stack (1–17), area 2 = stack (18–35), area 3 = stack (36–53), and area 4 = stack (54–72).

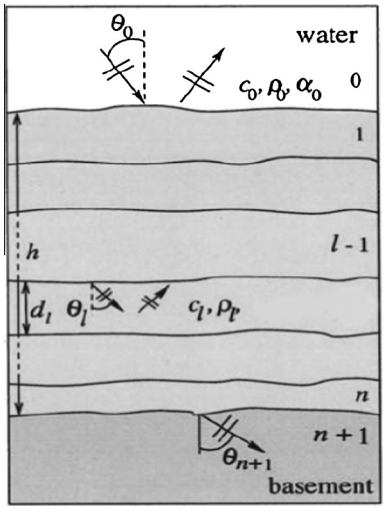

Figure 3 Theoretical sediment layer structure (Guillon and Lurton, 2001).

of consistency, the four calibration factors are averaged and used for the entire dataset.

The classification result as main grain size is shown in Fig. 2 in solid black, overlaid with classification using APL model (Applied Physics Laboratory, 1994) in cyan. The model was originally developed to simulate the SBES system that does account for backscatters. As depicted in Fig. 2, both results have a general agreement. In fact, the energy based model is more stable than the APL model. Visually, the APL classification at 'area 1' and 'area 2' has a more stochastic than at 'area 3' and 'area 4'. This comes from the contribution of backscatter; soft sediments have larger backscatter component than at rough sediments.

3.2. Sub-bottom classification

In this section, the low frequency 15 kHz echoes are analyzed to classify the sub bottom layers. Eq. (1) is only applicable for high frequency where the reflection component dominates the full

Table 1 Sediment absorption coefficients (Hamilton et al., 1982).

Sediment type	M_z (ϕ)	ρ (kg/m^3)	c (m/s)	α (dB/λ)
Clay	9	1.200	1.470	0.08
Silty clay	8	1.300	1.485	0.10
Clayey silt	7	1.500	1.515	0.15
Sand-silt–clay	6	1.600	1.560	0.20
Sand-silt	5	1.700	1.605	1.00
Silty sand	4	1.800	1.650	1.10
Very fine sand	3	1.900	1.680	1.00
Fine sand	2	1.950	1.725	0.80
Coarse sand	1	2.000	1.800	0.90

Table 2 Required variables to be estimated for nth layer.

Parameter	Number of required parameters
E_{TX}	1
Attenuation	$N + 1$
Transmission coefficient	$2N$

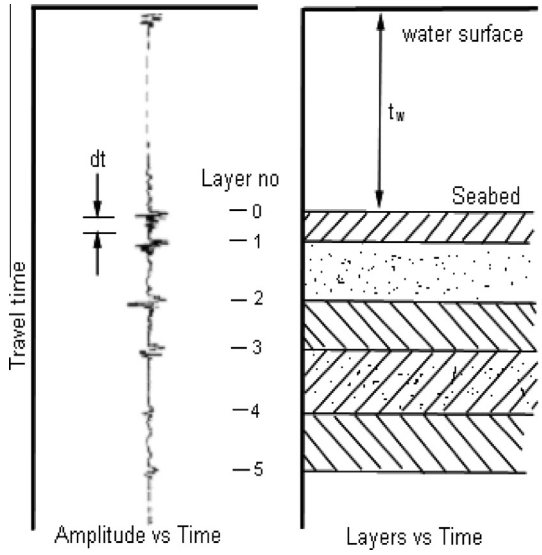

Figure 4 Physical reflection model (Caulfield and Yim, 1983).

echo profile. The low frequency is composed of multiple reflections from the deeper sediment layers. Thus, the energy model has to be extended to account for the further physical processes of layering absorptions, transmissions and reflections.

Consider a transmitted low frequency pulse emitted perpendicular toward a fluid dissipative sedimentary layer of thickness h and split into n elementary layers as in Fig. 3. Each layer l is characterized by its sound speed C_l, density ρ_l, attenuation coefficient α_l, and thickness d_l. During the travel time in the water column, the pulse gets weaken by the water absorption and spherical spread. Afterward the pulse encounters the first reflection at the water-seabed interface which is the highest reflection component due to the high impedance value. The remaining energy will penetrate inside the sediment layer with a transmission coefficient of T_{WS1} and subjected to a secondary spherical loss limited to the layer thickness d_l and its

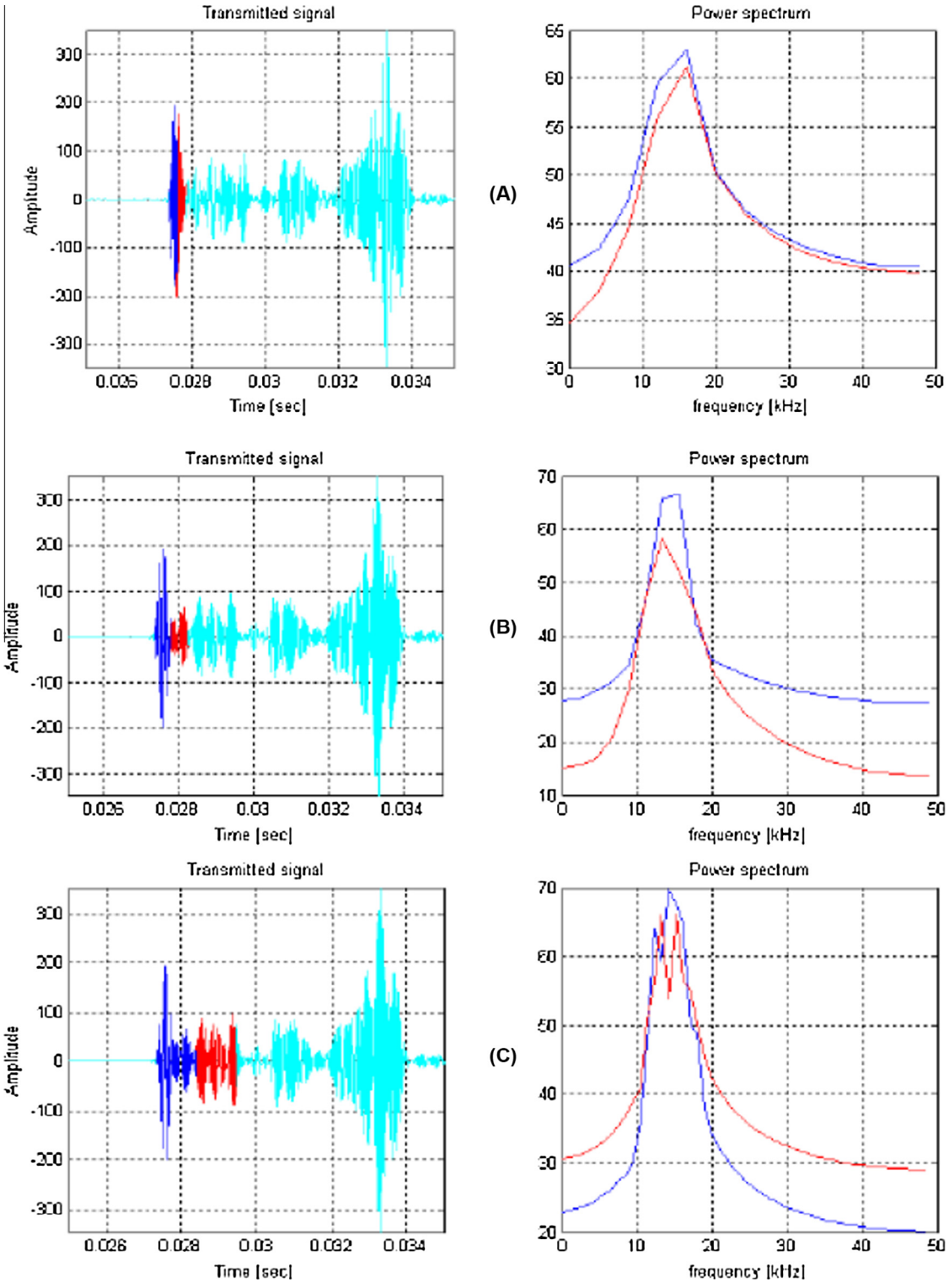

Figure 5 From top to bottom, sample size = 1 pulse width, 2 pulse width, and 4 times the pulse width.

corresponding sediment absorption. The absorption losses of the first layer should be estimated via the prior knowledge of the sediment type as proposed in the previous section or by any proper mean. The absorption coefficient of the first layer is estimated in Table 1 by the absorption coefficient in marine sediments equation:

$$\alpha = k \cdot f^n \tag{6}$$

where linear frequency dependent attenuation is considered, k = constant that depends on sediment type, f = transmitted frequency, and n = exponent of frequency dependence. Most authors support linear frequency dependent attenuation which

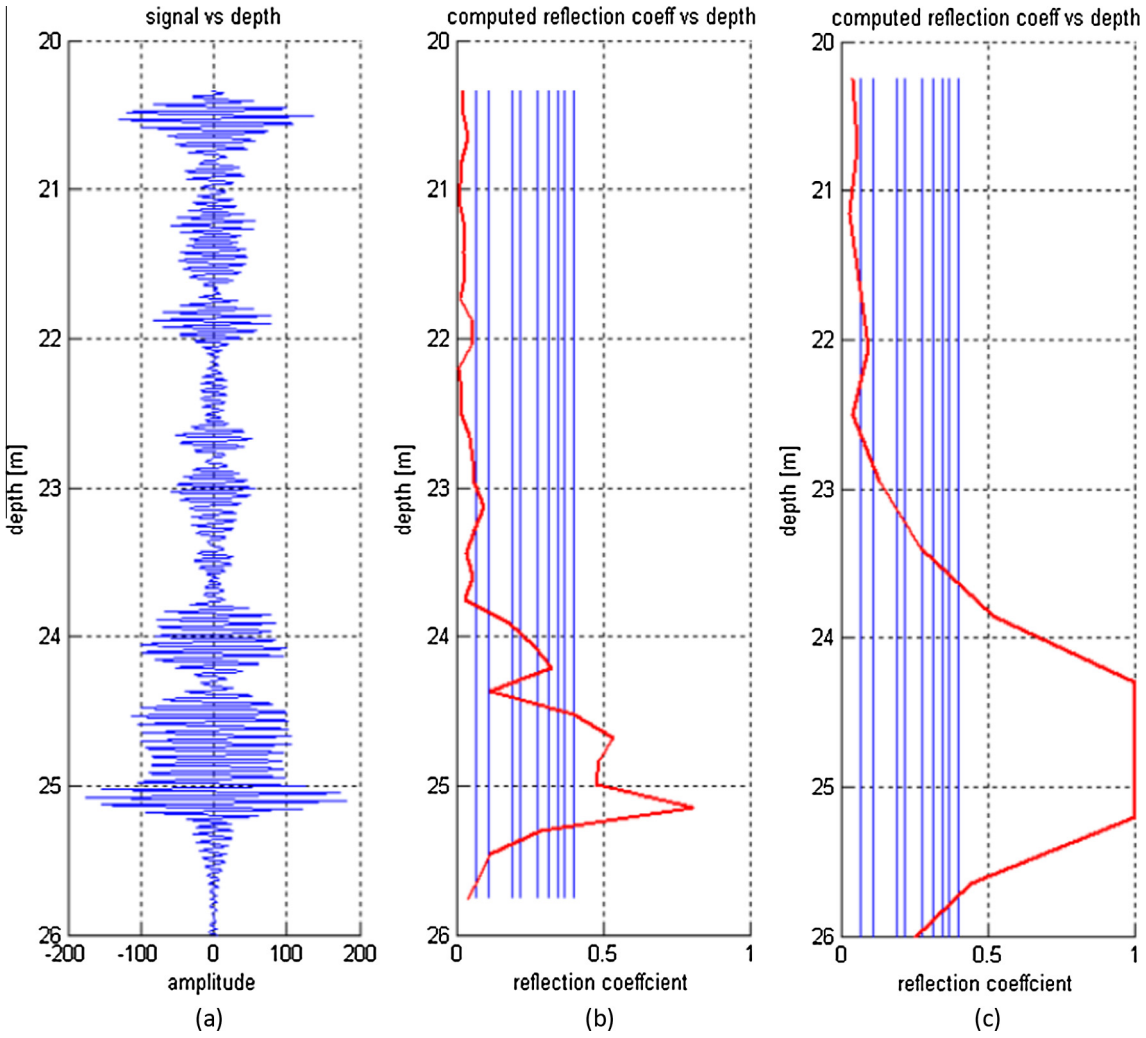

Figure 6 Comparison between sample size influences on the reflection coefficient estimates. (a) The received signal (area 1–15 kHz). (b) Estimated reflections, window size set two times the pulse length. (c) Estimated reflections, window size set to four times the pulse length.

is also followed in the current research by using Hamilton and Bachman's absorption values shown in Table 1. There is a variety of sediment absorption units that are commonly used in the underwater acoustics and marine seismology communities. Most common is the decibel per unit meter, or decibel per wavelength depending on the used propagation model. In Table 1 the acoustic attenuation α_l is expressed in decibel per wavelength so it can be used with any frequency. In the used model, the attenuation coefficient was converted to dB/m to agree with the units of the extended equation.

Once the pulse meets the second layer, a new reflected energy is born which is the impedance ratio between the first layer and second layer, subjected to attenuations of traveling way back to the receiver, which is the same as the transmission attenuations. After deducing the second reflection coefficient, the unknown impedance of the second layer is inversely estimated. The penetrated energy into the second layer will encounter the same physical processes until the energy vanishes or is completely reflected by a solid layer. The mathematical description of the mentioned process for two medium interfaces "water – 1st sediment layer" and "1st sediment layer–2nd sediment layer" is described through the following equation:

$$E_{RX} = E_{TX}\left(\frac{e^{(-4\alpha_w H)}}{4H^2}\right) T_{ws1}^2 \left(\frac{e^{(-4\alpha_{s1} d_1)}}{4d_1^2}\right) R_{s1s2}^2 T_{sw1}^2 \tag{7}$$

where α_{s_1} the acoustic attenuation due to sediment absorption at the first layer, d_1 is the thickness of the first layer, and $T_{ws1} = 1 + R_{ws1}$ is the transmitted energy coefficient from the water–sediment interface. The reflection coefficient at the boundary of the first and second layer is denoted by R_{s1s2}, and $T_{s1w} = T_{ws1}$ is the transmitted energy coefficient at sediment–water interface. The number of required parameters in the general expression depends on the number of layers (N). Table 2 shows the required number of parameters in order to compute the reflection coefficient at the corresponding layer.

3.3. Reflection calculation versus time

Fig. 4 illustrates a waveform of a shallow sub-bottom record with water depth travel time t_w and sample window dt. The sample window size is a very crucial factor to calculate proper and stable sequential reflection coefficients. A very short sample window will not capture the full reflected energy that represents the impedance contrast, while too large sample window

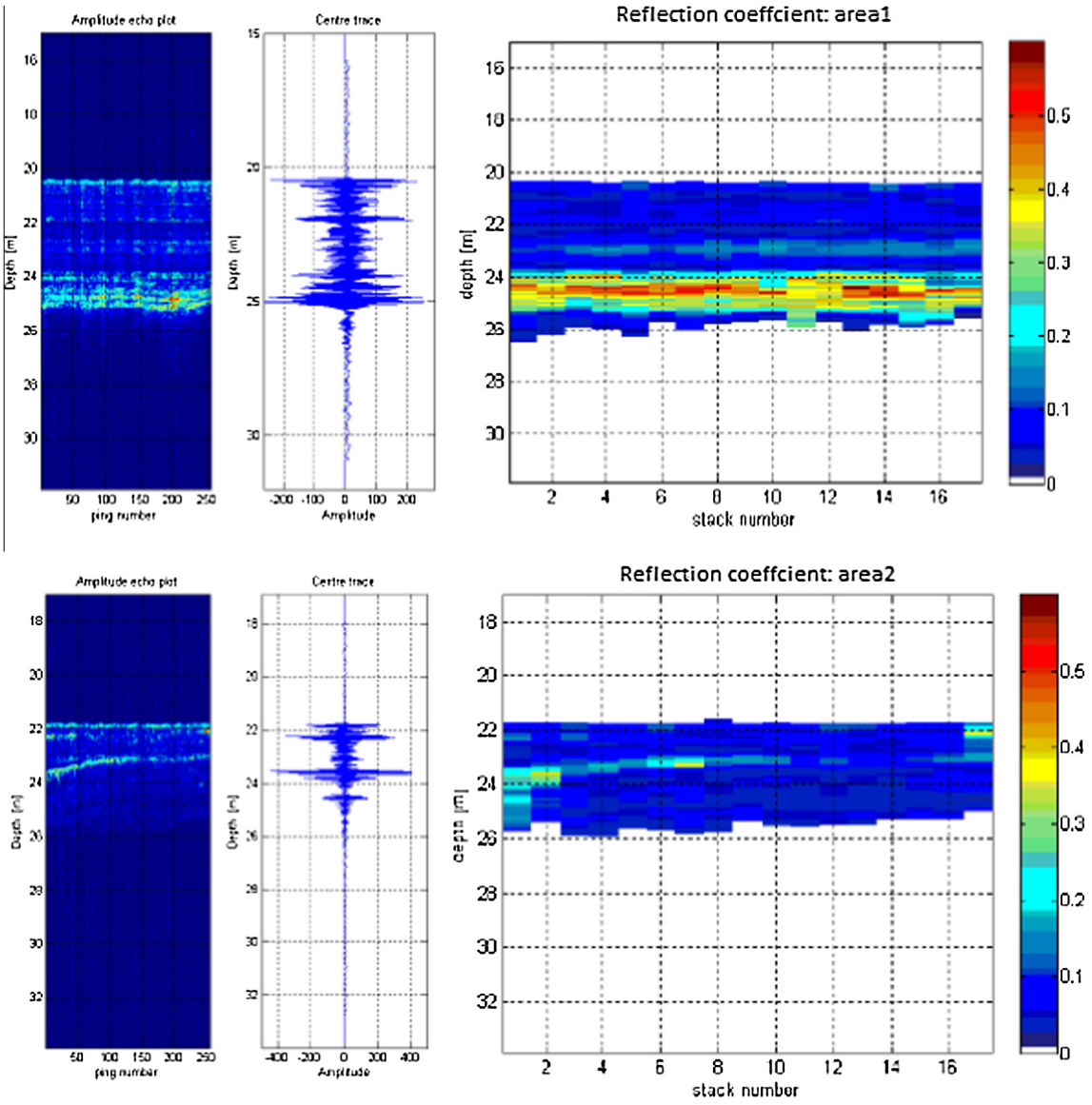

Figure 7a Raster plots of the estimated reflection coefficients at the first and second study areas.

will sum up multiple reflected energies of several layers. As a result the model will easily converge to improper reflection values and imbalance the full process. The principle of choosing proper sample window will be investigated in the next section. For now, the size of the sample window is chosen to be once or twice the transmitted pulse length as will be shown in the next section. The first reflected energy starts at t_w followed by N subsections of energy chunks $S(dt_1)$, $S(dt_2)$ … $S(dt_n)$. The energy profile versus time for each layer is described through the following equation:

$$E(t_n) = \sum_{t=t_1}^{t_2} (S(t))^2 \cdot dt_i \tag{8}$$

where:

$t_1 = t_w + \sum_{i=1}^{n-1} dt_n$
$t_2 = t_1 + dt_n$
t_w = water depth travel time.
dt_n = sample window of nth subsection.

3.4. Sample window size

The size of the sampling window is very crucial for the estimation of the local reflection coefficient. Basically too short sample window will not capture the correct energy that represents the desired local layer, while too large sample window will overestimate the reflection coefficient as it will overlap with the energy of the next layer. Keep in mind that calculating reflections coefficient versus depth is only valid when secondary reflections of the transmitted pulses are not located within the sampling window of the first arrival pulse. In order to evaluate this, a power spectrum analysis method is applied on two sequential sample windows. The method is basically inferred from the broadly used approach 'spectral ratio method' to estimate sediment absorption coefficients within homogeneous layer (Theuillon et al., 2008). It is based on the analysis of the frequency content of propagated acoustic waves. It is assumed that if the power spectrum of the second

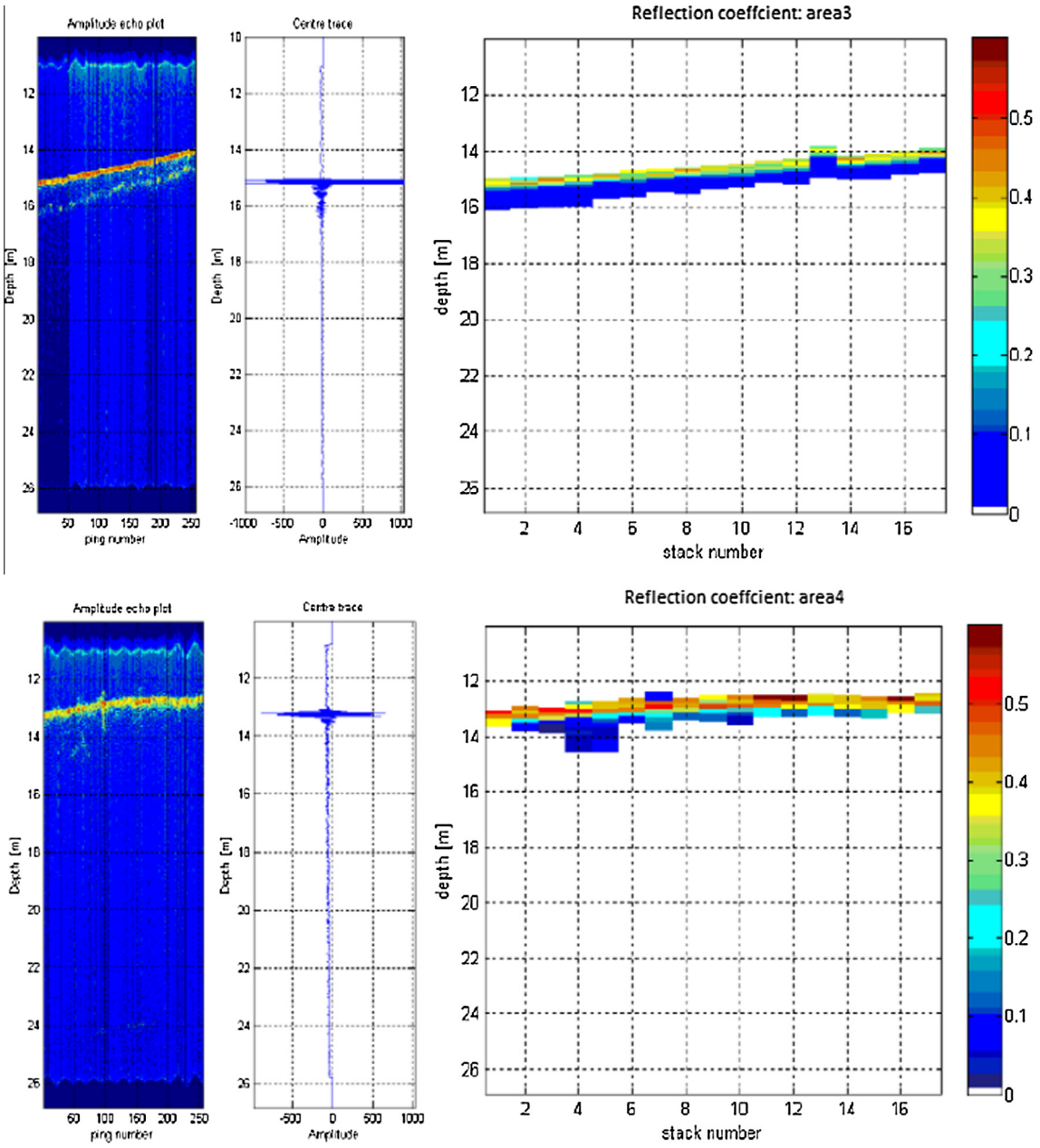

Figure 7b Raster plots of the estimated reflection coefficients at the third and fourth study areas.

sample window is the same or less than the power spectrum of the first sample window then we are at the same sediment layer. The power spectrum ratio of two sequential sample windows is depicted in Fig. 5 for 1, 2 and 4 times the transmitted pulse width. For the one time the pulse width, the spectrum profile was too coarse and difficult to compare. The two times the pulse width improved the spectral resolution and the comparison was applicable. Although the four times pulse width had the best spectral resolution, the comparison was not applicable since the sample window overlaps multiple reflections which unbalanced the time domain reflections.

The influence of the sample size selection on the reflection coefficients versus depth is illustrated in Fig. 6. In Fig. 6b, for a sample size equal to two times the pulse length, the reflection coefficients are consistent with the trend of the received signal. This behavior cannot be captured when the sample window was set to four times the band width as shown in Fig. 6c.

4. Classification results and discussion

Prior to any analysis, noise filtering and heave corrections are two essential steps to treat the stochastic behavior of the acquired dataset. The noise filtering was carried out by bandpass filter with center frequency similar to the transmitted frequency and proper bandwidth to conserve the signal shape properties. Although the data were heave compensated according to the values recorded from the heave sensor, some small heave variations remained. Basically, the heave effect causes stochastic variation in the echo shape, amplitude and time travel over consecutive pings. This behavior is removed by averaging a proper number of consecu-

tive pings to preserve its consistency. The group size was selected via the average highly cross correlated profiles; in the current research there were 15 pings.

4.1. Classification results

The classification results are plotted in Figs. 7a and 7b in terms of reflections. Reflections can easily be converted by empirically estimating the C value in Eq. (5). In general, the classification result in terms of reflection strength shows visual agreement with raw dataset. The surface classifications also agreed with the general discretion of the acquired areas.

4.2. Discussion

The extended classification model is an approximate estimate in the energy and time domain. For the energy domain multiple reflections were neglected. Multiple reflections can occur when a reflected signal is trapped between two layers 'i.e. delayed' and added to reflections that are encountered from deeper layers 'i.e. synchronized in time'. In this process, the received echo will be a component of amplitudes 'e.g. destructive and constructive' which will not represent the true sediment layer and consequently will degrade the reflection coefficient results. Volume backscatter is also important to be considered especially at thick soft sediment layers. Regarding the time domain, the windowing sample can be replaced by cross correlation to compute distinct layer depths with homogeneous sediment characteristics.

5. Conclusion

Remote classification of sub-bottom layers is vital of importance for many engineering and marine applications. Physics based models are of high demand to save the effort of boreholes investigations. An energy model initially implemented for surface classification using high frequency signals was extended to account for sub-layer interactions using low frequency echoes. Echoes come from sub-layers by a series of reflections at sub layer interface with high impedance. The model estimates the reflection coefficients inversely via transmitted and received echo energies. The model incorporates a number of losses and physical interactions such as spherical spread losses, water and sediment attenuations, reflections and refractions coefficients. The energy values are estimated in the time domain via sequential time window. The size of the time window is crucial factor on the model stability.

The classification result agreed with the visual inspection of the area Corse samples. Unfortunately, no laboratory results were available to evaluate the classification quantitatively. The model is very sensitive to the presence of errors. The errors might appear from absorption factors that are deviated from the true value, or even misclassified layers. These errors are acceptable at the first couple of layers, and can increase drastically by increasing the layer index.

Resolution is a crucial issue, if low resolution is used 'i.e. large sample window', the reflection predictions will be inaccurate, by missing intermediate layers. This inaccuracy will behave as an error which will propagate within the second iteration and will influence the reflection predictions of the following sample windows. Therefore, a proper sample window has to be chosen to capture the full reflected energy from the desired layer and without overlapping with secondary reflections.

The extended model is an approximate estimate that can be enhanced to include confined reflections and volume backscatter of thick soft sediments. The energy simulation can be enhanced by computing correct layer depths to replace the sampling window method.

References

Anderson, J.T., Van Holliday, D., Kloser, R., Reid, D.G., Simard, Y., 2008. Acoustic seabed classification: current practice and future directions. ICES J. Mar. Sci. 65, 1004–1011.

Applied Physics Laboratory, University of Washington, 1994. APL-UW High-Frequency Ocean Environmental Acoustic Models Handbook, Seattle, WA, Tech. Rep. TR-9407.

Caulfield, D.D., Yim, Yung-Chang, 1983. Prediction of shallow sub-bottom sediment acoustic impedance while estimating absorption and other losses. J. Canad. Soc. Explor. Geophys.

Chivers, R.C., Emerson, N., Burns, D., 1990. New acoustic processing for underway surveying. Hydrogr. J. 42, 8–17.

Eleftherakis, Dimitrios, AliReza, Amiri-Simkooei, Snellen, Mirjam, Simons, Dick G., 2012. Improving riverbed sediment classification using backscatter and depth residual features of multi-beam echo-sounder systems. Acoust. Soc. Am.

Garrison, G.R., Francois, R.E., 1879. Sound absorption based on ocean measurements. Part II: Boric acid contribution and equation for total absorption. J. Acoust. Soc. Am. 72 (6), 1879–1890.

Guillon, Laurent, Lurton, Xavier, 2001. Backscattering from buried sediment layers: The equivalent input backscattering strength mode. J. Acoust. Soc. Am. 109 (1), 122–132.

Hamilton, E.L., Bachman, R.T., Berger, W.H., Johnson, T.C., Mayer, 1982. Acoustic and related properties of calcareous deep-sea sediments. LA: Petrol 52, 733–753.

Heald, G.J., Pace, N.G., 1996. An analysis of the 1st and 2nd backscatter for seabed classification. In: European Conference on Underwater Acoustics, 24–28 June 1996. vol. II, pp. 649–654.

Hughes Clarke, J.E., Danforth, B.W., Valentine, P., 1997. Areal seabed classification using backscatter angular response at 95 kHz. Lerici, Italy: High Frequency Acoustics in Shallow Water, NATO SACLANT Undersea Research Centre, 30 Jun-4 Jul 1997. Vol. Series CP-45, pp. 243–250.

Lurton, X., 2002. An Introduction to Underwater Acoustics: Principles and Applications. Springer, Praxis, Chichester, UK.

Orłowski, A., 1984. Application of multiple echoes energy measurement for evaluation of bottom type. Oceanologia 19, 61–78.

Preston, J.M., Christney, A.C., Beran, L.S., Collins, W.T., 2004. Statistical seabed segmentation e from images and echoes to objective clustering. In: Proceedings of the Seventh European Conference on Underwater Acoustics.

Siwabessy, P.J.W., Penrose, J.D., Kloser, R.J., Fox, D.R. 1999. Seabed habitat classification. In: Proc. International Conference on High Resolution Surveys in Shallow Waters DSTO, 18–20 October 1999, Sydney, Australia.

Sternlicht Daniel, D., De Moustier Christian, P., 2003. Time-dependent seafloor acoustic backscatter (10–100 kHz). Acoust. Soc. Am.

Theuillon, G., Stéphan, Y., Pacault, A., 2008. High-resolution geoacoustic characterization of the seafloor using a subbottom profiler. IEEE J. Ocean.

Urick, R.J., 1982. Sound Propagation in the Sea. Peninsula Publishing, Los Altos, California, Vol. 212 pp.

Van Walree, Paul A., Ainslie, Michael A., Simons, Dick G., 2006. Mean grain size mapping with single-beam echo sounders. J. Acoust. Soc. Am. 120 (5), 2555.